1st AIAA Atmospheric and Space Environments Conference
22 - 25 June 2009, San Antonio, Texas

AIAA 2009-4259

Prediction of Propeller Performance in Icing Conditions using Vortex Theory

Greg Busch,[1] Michael Bragg,[2]
University of Illinois at Urbana-Champaign, Urbana, IL 61801
and
Andy Broeren[3]
NASA Glenn Research Center, Cleveland, Ohio 44135

A vortex theory propeller code was developed and validated using experimental data from a previous full-scale propeller test to analyze propeller performance in icing conditions. The code used propeller geometry and blade section aerodynamic performance data as inputs to compute propeller thrust and power coefficients. After initial validation, the code was applied to a different propeller for which clean and iced thrust data were recently acquired in the McKinley Climatic Laboratory. During the McKinley test, ice accretions were documented, allowing iced blade-section aerodynamic performance data to be obtained experimentally in the University of Illinois 15" x 15" wind tunnel by using ice simulations. These blade-section performance data are discussed in detail in this paper. Using these data, the propeller code predicted thrust and efficiency reductions and changes in required power comparable to those measured in the McKinley test for Appendix C icing conditions. Ice shedding was found to be significant for SLD icing conditions and it is recommended that a shedding model be developed and implemented in the propeller performance code to more accurately predict performance degradation in such conditions.

Nomenclature

α	angle of attack
α_i	induced angle of attack
b	airfoil model span
β	blade pitch angle
B	number of propeller blades
c	airfoil chord length
C_d	drag coefficient
$C_{d,min}$	minimum drag coefficient
C_l	lift coefficient
$C_{l,max}$	maximum lift coefficient
C_P	propeller power coefficient
C_T	propeller thrust coefficient
D	propeller diameter
dC_P	incremental power coefficient at a single blade section
dC_T	incremental thrust coefficient at a single blade section
η	propeller efficiency
J	propeller advance ratio
k	ice feature height
LWC	liquid water content
M	freestream Mach number
MVD	median volume diameter of water drops
OAT	outside air temperature

[1] Graduate Research Assistant, Department of Aerospace Engineering, Member AIAA
[2] Professor of Aerospace Engineering, Executive Associate Dean for Academic Affairs, Fellow AIAA.
[3] Aerospace Engineer, Icing Branch, Previously Research Scientist, University of Illinois at Urbana-Champaign, Associate Fellow AIAA.

Re	freestream Reynolds number, based on the airfoil chord length
r	coordinate in the propeller radial direction
R	propeller radius
σ	blade solidity, $Bc/(\pi R)$
s	airfoil model coordinate along the surface length
SLD	super-cooled large droplet
w	induced velocity at propeller blade section
V_E	resultant velocity seen by propeller blade section
x	non-dimensional radial station, r/R
z	coordinate in the airfoil model spanwise direction

Introduction

Ice accretion on propeller blades can cause considerable losses in propeller thrust and efficiency. Recently the FAA has investigated propeller performance degradation due to icing conditions using a combination of experimental and computational methods. The current study builds on work done recently at the McKinley Climatic laboratory on a full-scale propeller.[1]

Propeller performance degradation due to icing conditions has been investigated in past studies. In 1946, Corson and Maynard[2] simulated ice accretion on a 10-ft. diameter propeller and measured propeller thrust and efficiency in the NASA Langley 16-ft. high speed tunnel. Lacking data from a propeller icing test, the artificial ice shapes were based on wing icing data. The shapes caused decreases in propeller efficiency of up to 3%. Two years later, Preston and Blackman[3] conducted flight tests in natural icing conditions and documented typical efficiency losses of about 10%. In more severe cases, they recorded efficiency decreases of up to 19%. In 1950, Neel and Bright[4] conducted additional flight tests and measured similar reductions in efficiency. To complement these tests, they developed a propeller analysis code using blade-element theory; this code predicted performance penalties similar to those observed during the flight tests. Neither of these latter studies thoroughly documented the ice accreted during the flight tests.

In 1984, Korkan et al.[5] developed a theoretical model for analyzing propeller performance and were able to obtain good agreement with published experimental data. Another analytical model, an enhanced strip method, was developed by Miller et al.[6] This code used Bragg's 2-D droplet trajectory code[7] to calculate the accumulation parameter and collection efficiency, and empirical correlations of Gray,[8] Bragg,[5] and Flemming[9] to determine the effect of ice accretion on blade section performance. Since the Bragg and Gray correlations dealt only with C_d, a reduction in lift of 5% was assumed (relative to the clean value). It was found that analytical predictions of propeller performance agreed with the experimental measurements by Neel and Bright[4] to within the uncertainty of the correlations. It was also found that the output of the code depended substantially on the correlation used.

Reichhold et al.[10] used blade-element theory to explain how droplet impingement efficiencies greater than one could occur for propellers. Farag and Bragg[11] developed a three-dimensional droplet impingement code to determine the magnitude of three-dimensional effects on droplet trajectories in the vicinity of a propeller. The authors found that the number of propeller blades did not have a large effect on impingement characteristics, but the propeller power setting and nacelle/spinner geometry had a substantial effect. The code was again validated using three-dimensional experimental data and two-dimensional computational data which had been corrected for three-dimensional effects, and best agreement occurred when the spinner/nacelle was non-existent or very small. These studies show that two-dimensional strip methods can provide accurate results, although they may be affected by spinner/nacelle effects.

Most recently, during an icing flight test of an MU-2B, propeller ice accretion caused airspeed to drop by over 40 kts,[12] prompting Dumont et al.[1] to conduct an icing wind tunnel test to document propeller ice accretion and the associated reduction in thrust. The test was conducted at the McKinley Climatic Laboratory on a full-scale, 8-ft. diameter propeller. Ice accretions were documented using stop-action video during the test and with tracings after the test. Three tracings were taken along the propeller blade, at the 25% (mid-boot), 50%, and 75% radial stations. Still photographs were taken at the end of each test run for each accretion. The reduction in propeller thrust was also documented by taking measurements of thrust before and after the application of the icing cloud. Reductions in thrust averaged 5.9% and 13.4% for Appendix C and SLD conditions, respectively. The maximum measured thrust reduction was 21.2% in SLD conditions.

The objective of the current research program is to develop a methodology to analyze propeller performance in icing conditions. This objective will be achieved using both experimental and computational methods. A propeller

performance code has been developed to predict propeller performance given the aerodynamic performance characteristics of the propeller blade sections. These performance characteristics were obtained by simulating the ice accretions of the test by Dumont et al.[1] on airfoils in the Illinois wind tunnel and input into the code. The propeller performance data measured by Dumont et al.[1] were used to determine the accuracy of the propeller code. This process is documented in this paper. Future extensions of this work include integration of LEWICE and a planned 2-D RANS code and are briefly described in the conclusions section.

This paper is divided into four additional sections. The following section discusses the development of the propeller code and describes a validation case. The Experimental Methods section gives an overview of the methods used to obtain iced-airfoil aerodynamic performance data for use with the propeller code. The Results section presents propeller performance calculations obtained from the propeller performance code and compares this calculated performance to experimental data. The final section presents the key results and conclusions of this study.

Propeller Performance Code

This section first gives a brief overview of the basic theory and assumptions used to develop a propeller performance code. It then explains how the code was validated, using experimental data from an icing test on a full-scale propeller.

Theory

To complete the computational portion of this study, a propeller performance code was developed using the blade-element and vortex theory methods described by McCormick.[13] Blade-element theory discretizes the propeller blade radially into thin blade sections; the geometry of one such section is shown in Fig. 1. Given the propeller geometry and the aerodynamic performance characteristics of each blade section, the incremental thrust and power coefficients dC_T and dC_P can be obtained as a function of known quantities and the induced angle of attack α_i on each blade section (eqns. 1 and 2). Once the induced angle of attack is known, the incremental thrust and power coefficients can be integrated across the propeller blade and multiplied by the number of blades to compute the propeller thrust and power coefficients.

$$dC_T = (J^2 + \pi^2 x^2)\sigma[C_l \cos(\phi + \alpha_i) - C_d \sin(\phi + \alpha_i)] \tag{1}$$

$$dC_P = \pi x(J^2 + \pi^2 x^2)\sigma[C_l \sin(\phi + \alpha_i) + C_d \cos(\phi + \alpha_i)] \tag{2}$$

Vortex theory is used to obtain the induced angle of attack on each blade section. The theory assumes that the propeller blade trailing vortices lie along a helical path of constant pitch in the propeller ultimate wake. Combining this assumption with the Kutta-Joukowski theorem and a second assumption that the induced velocity w is normal to the resultant velocity V_E (Fig. 1), the induced velocity (and thus α_i) at each blade section can be related to the local section lift coefficient C_l. However, since C_l is dependent on α_i, an iterative scheme is necessary to solve for α_i. Once α_i is known, blade-element theory provides C_T and C_P, as described above. Note that tip losses are accounted for using Prandtl's tip-loss factor, which drives the section lift coefficient to zero at the blade tip. More details of this code are documented by Krug.[14]

Validation – Clean Propeller

The propeller performance code was validated using data from Corson and Maynard,[2] who, as discussed in the Inroduction, conducted a test campaign on a full-scale, 10 ft. diameter Curtiss propeller in the Langley 16-ft. high-speed tunnel. The propeller blades consisted of Clark Y airfoil sections, and the chord, thickness, and twist distributions along the blade were documented. Corson and Maynard[2] measured the effects of simulated ice on propeller efficiency and thrust and power coefficients at multiple advance ratios (J) using a propeller dynamometer. The approximate location of the simulated ice is shown in Fig. 2.

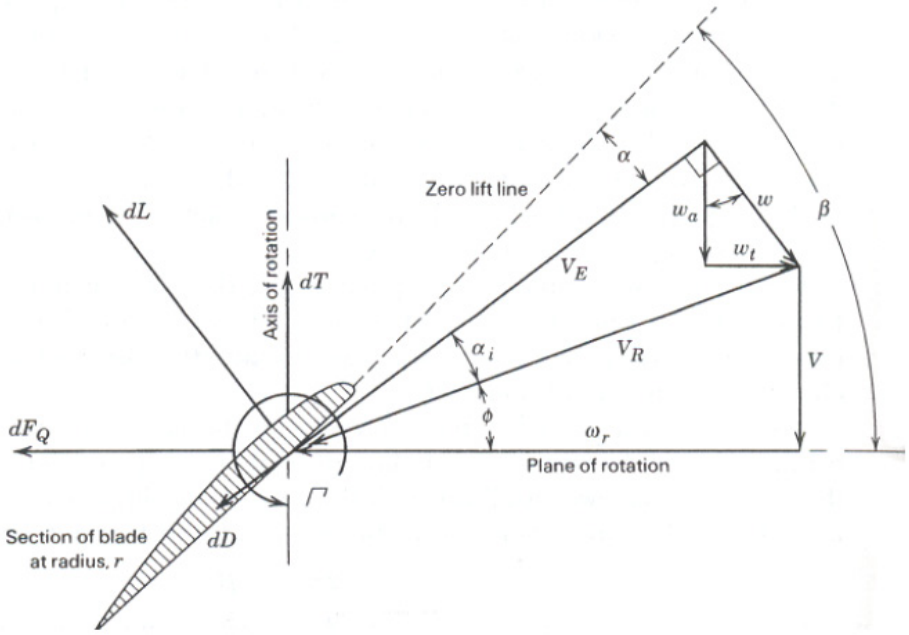

Fig. 1 Geometry used in development of the propeller performance code (adapted from McCormick[13]).

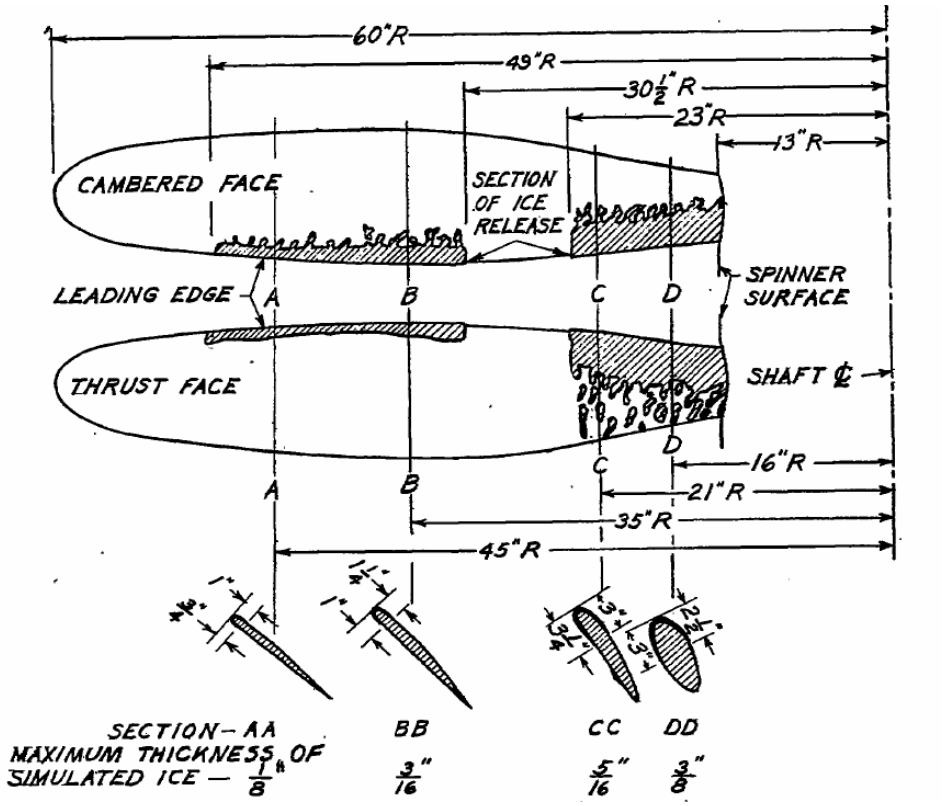

Fig. 2 Approximate location and size of ice simulations used by Corson and Maynard.[2]

To analyze the Curtiss propeller using the propeller performance code, each blade was discretized into seven sections. The blade chord, thickness, and twist at the center of each section was calculated using the geometry distributions provided by Corson and Maynard,[2] and XFoil[15] was used to obtain the aerodynamic performance of

each section at the appropriate local Mach and Reynolds numbers (assuming standard conditions). At some of the advance ratios used by Corson and Maynard,[2] the local Mach number near the blade tip approached 0.8. XFoil was unable to correct for compressibility at such a high Mach number at higher angles of attack. Therefore, data at these blade stations were obtained near $\alpha = 0$ deg. and extrapolated linearly. Using these extrapolated data, the code computed a local angle of attack below 4 deg. at the outboard blade stations for all advance ratios, so the extrapolation was considered to be reasonable. Once the aerodynamic performance data for each of the seven blade sections were obtained, they were interpolated along the blade radius (based on airfoil thickness) to account for the continually varying blade thickness and local Mach and Reynolds numbers.

The clean Curtiss propeller performance predicted by the propeller performance code is compared with that measured by Corson and Maynard[2] in Fig. 3. Overall agreement in thrust coefficient is good, although the slope of the C_T curve predicted by the code is slightly more negative than that measured experimentally. The code under-predicts C_P at low and high advance ratios but is fairly accurate at moderate advance ratios. The code of Miller et al.[6] also under-predicted C_P, although it did so at all advance ratios. The under-prediction of C_P may in part be due to the fact that C_P is more dependent than C_T on blade section C_d. There is generally more uncertainty associated with the quantification of airfoil C_d than C_l (especially when using a program such as XFoil, as used here), since effects such as surface roughness and flow conditions have a larger effect. Since the value of C_d is significant when calculating C_P, this uncertainty manifests itself in predictions of C_P. The under-prediction of C_P results as an over-prediction of propeller efficiency, as shown in Fig. 3(c). The code predicts the propeller's peak efficiency at $J = 0.8$ to be about 9% and 6% higher than the experiment at pitch angles of $\beta = 20$ and 25 deg., respectively.

Note that C_T and C_P are very sensitive to changes in propeller pitch. Recall that the data shown in Fig. 3 were based on the twist distribution given by Corson and Maynard.[2] These data were given in graphical format, so the exact twist distribution could not be determined. The thrust and power coefficient curves presented in Fig. 3 were generated from twist data which were adjusted within the uncertainty of the graph given in the report to obtain good agreement.

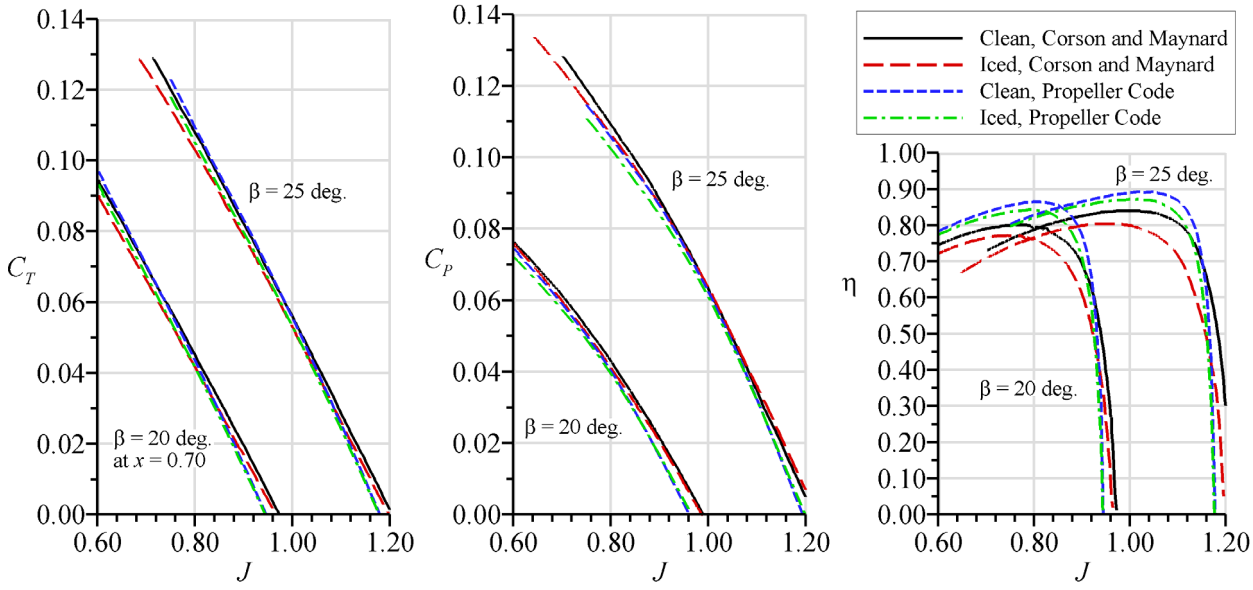

Fig. 3 Comparison of propeller (a) thrust coefficient, (b) power coefficient, and (c) efficiency computed by propeller code with experimental data taken from Corson and Maynard.[2] Data shown for two pitch angles: $\beta = 20$ deg. and $\beta = 25$ deg. at $x = r/R = 0.70$.

Validation – Iced Propeller

To account for the effects of the simulated ice accretion in the propeller performance code for this validation case only, lift and drag of the clean blade sections were penalized based on data from previous aerodynamic performance measurements on iced airfoils. For radial stations inboard of $x = 0.38$ and from $x = 0.51 - 0.82$ (the locations of the simulated ice accretion in Fig. 2), the iced blade section lift curve slope was assumed to be reduced to 90% of the value of the clean lift curve slope, and the iced blade section drag coefficient was assumed to increase

to 170% of the clean value. This estimated reduction in lift and increase in drag was used only to validate the propeller performance code; results of the code presented later in this paper are based on experimentally obtained iced-airfoil performance data. The propeller performance code results are compared to the data of Corson and Maynard[2] in Fig. 3. The propeller performance code predicts the ice accretion to cause very similar penalties to those observed by Corson and Maynard,[2] reducing C_T and C_P at low advance ratios but having a smaller effect at high advance ratios. These trends are consistent with those observed by Neel and Bright[4] during a flight test through icing conditions. Reductions in peak efficiency predicted by the propeller performance code are about 2% and 3% for the 20 and 25 deg. pitch angles, respectively, compared with the experimentally measured reductions of 4% and 5%.

Fig. 4 Wake rake installed behind 50% blade section airfoil model with ice simulation of Run 19A installed on leading edge.

The remainder of this paper discusses the use of the propeller performance code to analyze an 8-ft. diameter propeller used in a full-scale icing test at the McKinley Climatic Laboratory.[1] As discussed in the Introduction, propeller thrust measurements were obtained before and after the propeller was exposed to simulated icing conditions in an open-jet icing wind tunnel. The next section of the paper discusses the experimental methods to obtain aerodynamic performance data for iced and clean blade sections of the propeller, and the Results section reports performance predictions of the propeller code and presents a comparison with experimental thrust reduction measurements taken during the McKinley test.

Experimental Methods

The experimental component of this study was carried out at the University of Illinois. Aerodynamic testing was conducted in a subsonic, open-return wind tunnel which had a test section measuring 15 in. high, 15 in. wide, and 48 in. long. Inlet flow was conditioned using a four-inch honeycomb and four anti-turbulence screens. The tunnel was capable of achieving test section speeds of up to 350 ft/s, corresponding to a maximum Mach number of 0.3.

Three aluminum airfoil models, corresponding to the mid-boot, 50%, and 75% radial station blade sections on the propeller used by Dumont et al.,[1] were used in this investigation. The mid-boot radial station corresponded to the 25% blade section. Each airfoil model had a chord of 5.38 in and a span of 14.9 in. The mid-boot blade section was approximately 33% thick, the 50% blade section was 9% thick, and the 75% blade section was 6% thick. The 50% and 75% blade section airfoils were instrumented with 26 surface static-pressure taps, while the mid-boot blade section airfoil had 33 taps. Testing was performed at nominal conditions of M = 0.20 and M = 0.30, corresponding to chord Reynolds numbers of 600,000 and 900,000, respectively.

All pressures reported in this paper were measured using an electronically scanned pressure system. Lift and pitching moment coefficient data were obtained by integrating the measured surface pressures around the airfoil model. A wake rake, located 1.2 chord lengths downstream of the airfoil model in the center of the tunnel, was used to calculate the drag coefficient using standard momentum-deficit methods. The wake rake had 59 total pressure probes over a 9.72 in. span and three static pressure probes spaced 4.86 in. apart. Total pressure probes near the center of the rake had closer spacing than those near the ends. The wake rake is shown installed behind the airfoil model in Fig. 4. Note that C_d measurements were acquired at only one spanwise station due to time constraints, but Busch et al.[16] found that for some two-dimensional ice simulations, C_d may vary by up to 15% along the airfoil span.

As discussed in the Introduction, Dumont et al.[1] conducted a full-scale propeller icing test in the McKinley Climatic Laboratory and thoroughly documented ice accretions formed at the 25% (mid-boot), 50%, and 75% blade stations for several run conditions. Three of these run conditions, listed in Table 1, were chosen to validate the propeller performance code discussed above. Note that the McKinley test was conducted at a freestream velocity of 100 kts, which is substantially below the freestream velocity for in-flight conditions. Therefore, the flight-condition

blade section angle of attack could only be matched at a single radial station. This target angle of attack and the corresponding test location are given in Table 1. The conditions of Runs 3B and 19A are Appendix C conditions, while Run 21 is an SLD condition. Fig. 5 shows the ice accretion photos and tracings taken from Dumont et al.[1]

Table 1 Summary of run conditions used by Dumont et al.[1] for which ice accretions were simulated in the present study.

Run	LWC (g/m^3)	MVD (μm)	OAT (F)	Spray Time	Target α (deg)	Radial Location of Target α	Pitch, x = 0.61 (deg)	Torque (%)	RPM
3B	0.33	16.5	4.6	4 min 15 s	0.5	0.75	26.2	34	1480
19A	0.10	40	12.0	15 min 1 s	2.0	0.25	26.2	35	1535
21	0.36	96	12.0	11 min 30 s	2.0	0.25	25.1	23	1450

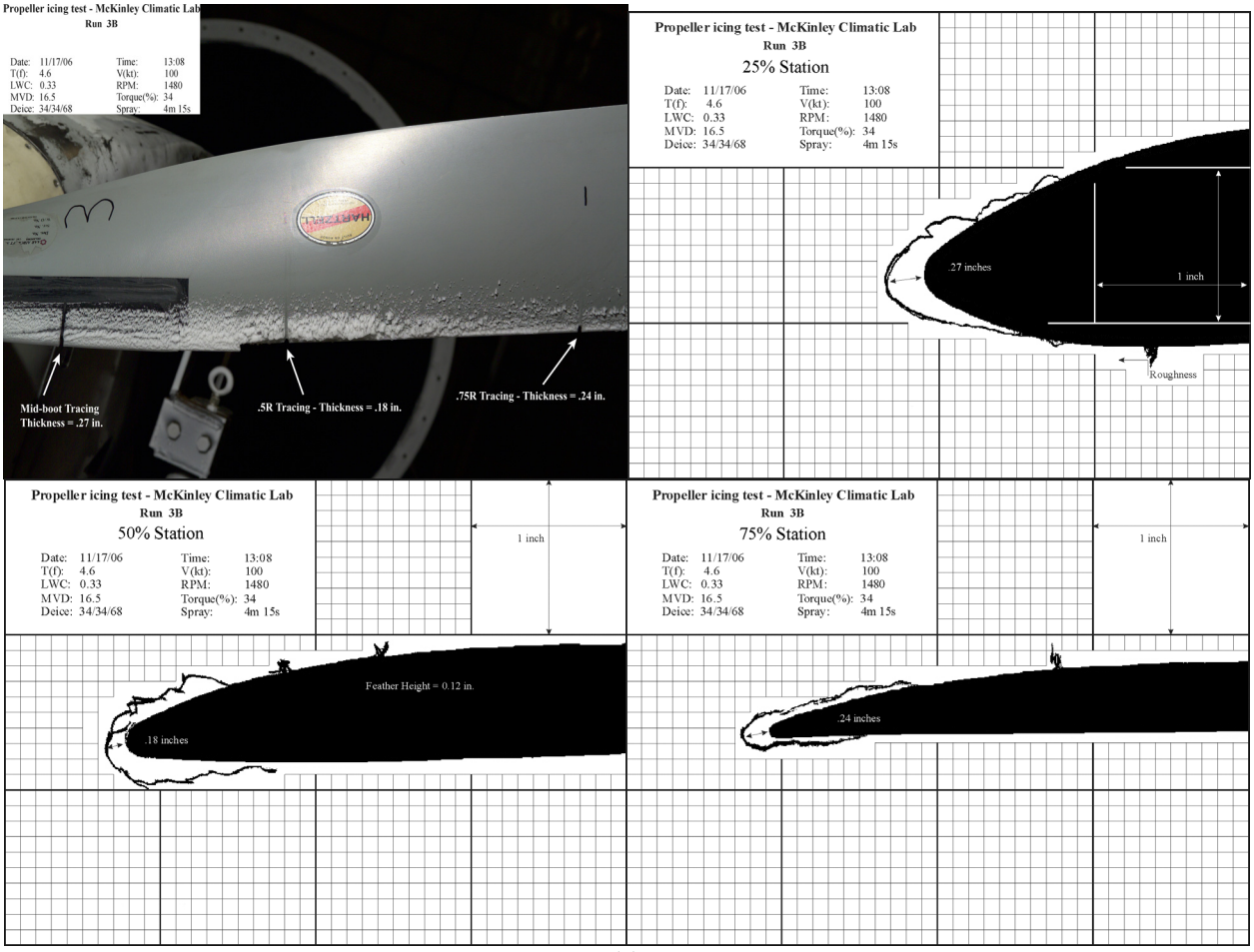

(a)

Fig. 5 Photos and tracings of ice accretions documented by Dumont et al.[1] These ice accretions were simulated in the Illinois 15 in. x 15 in. wind tunnel. The three tracings are for the propeller 25% (mid-boot), 50%, and 75% blade sections for the conditions of (a) Run 3B, (b) Run 19A, and (c) Run 21. (cont'd)

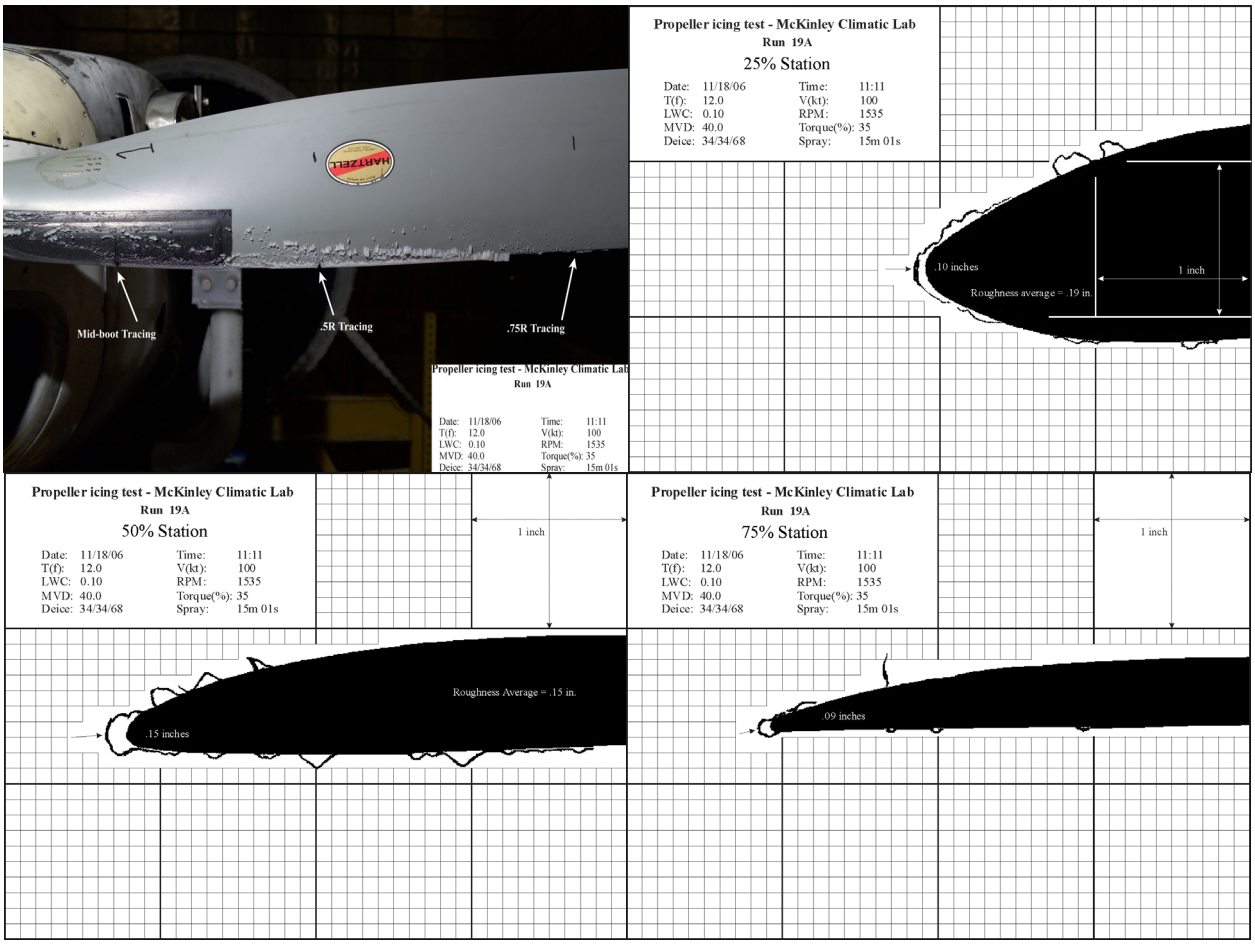

(b)

Fig. 5 Photos and tracings of ice accretions documented by Dumont et al.[1] These ice accretions were simulated in the Illinois 15 in. x 15 in. wind tunnel. The three tracings are for the propeller 25% (mid-boot), 50%, and 75% blade sections for the conditions of (a) Run 3B, (b) Run 19A, and (c) Run 21. (cont'd)

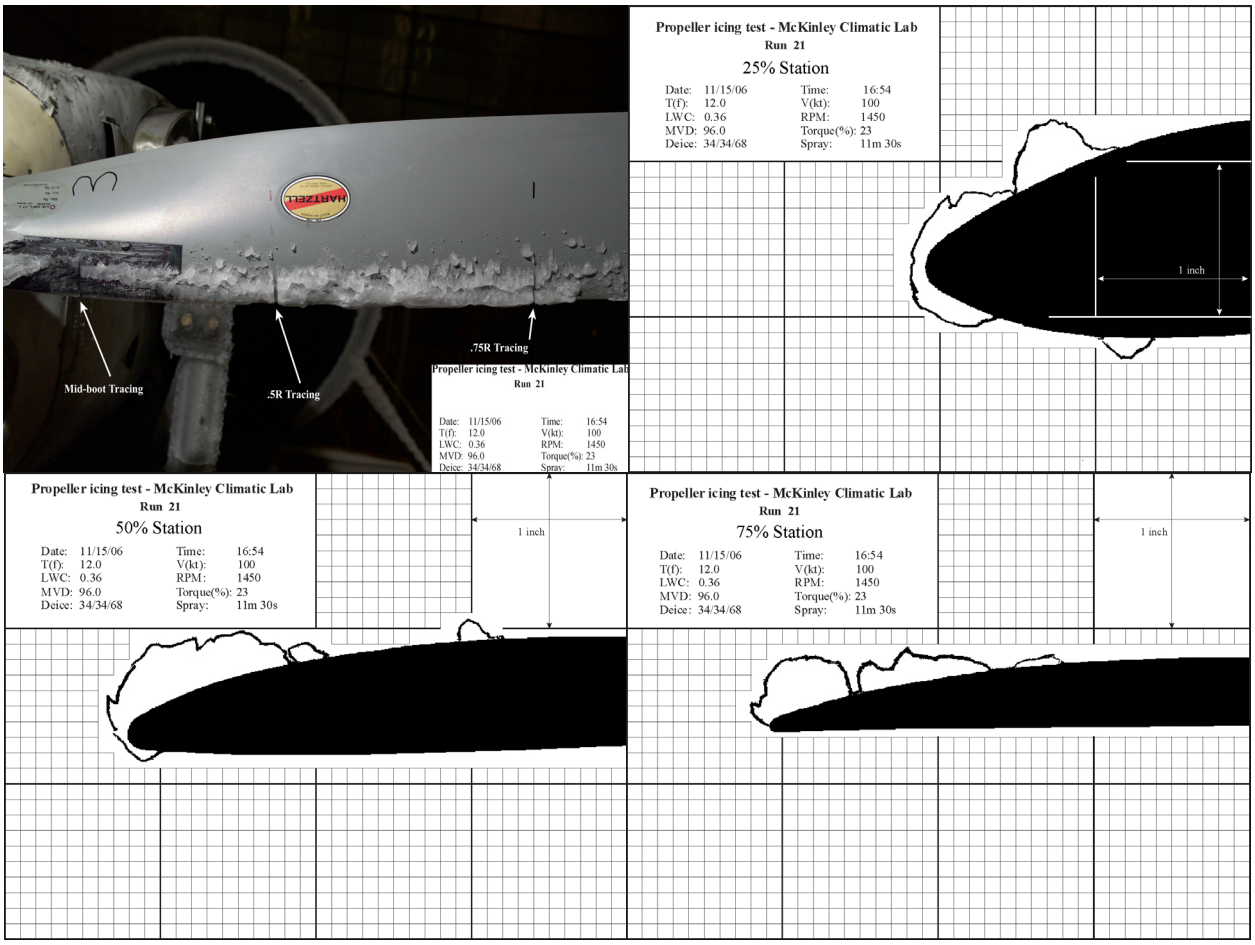

(c)

Fig. 5 Photos and tracings of ice accretions documented by Dumont et al.[1] These ice accretions were simulated in the Illinois 15 in. x 15 in. wind tunnel. The three tracings are for the propeller 25% (mid-boot), 50%, and 75% blade sections for the conditions of (a) Run 3B, (b) Run 19A, and (c) Run 21. (concluded)

The tracings shown in Fig. 5 were used to design simple-geometry ice accretion simulations for accretions corresponding to the conditions of Runs 3B, 19A, and 21. Past studies have shown simple-geometry simulations to provide reasonable estimates of C_l and C_d of the iced-airfoil, provided care is taken to accurately represent the accretion geometry.[17,18,19,20] The artificial ice shapes corresponding to the conditions of runs 3B and 21 were constructed from simple materials. Surface roughness was applied on top of the shapes using size k/c = 0.0031 aluminum oxide roughness elements and a 0.003-in. thick removable vinyl film. For the simulations corresponding to the conditions of Run 19A, larger walnut shell roughness elements (k/c = 0.017) were applied directly to the airfoil surface, as the ice accretions generated under these conditions were sufficiently small that no underlying geometry was necessary. Most of the simple-geometry simulations had no surface static-pressure taps. In some cases, however, an ice simulation would cover the airfoil model pressure taps. In these cases, the artificial ice shapes were instrumented with new pressure taps.

Results

The results section of this paper is divided into two parts. The first part discusses clean and iced aerodynamic performance of the 25% (mid-boot), 50%, and 75% propeller blade sections. The second part discusses propeller performance calculations made using these aerodynamic performance data and the propeller performance code discussed earlier in the paper.

Propeller Blade Section Aerodynamic Testing

Clean and iced aerodynamic performance data for each of the three propeller blade sections are shown in Fig. 6. The clean mid-boot blade section had $C_{l,max}$ = 1.19 at α = 14 deg. and C_d remained relatively constant around 0.018 from α = -5 to 12 deg. However, this airfoil section showed extreme sensitivity to surface contamination. A two-dimensional trip strip 1/8 in. wide and 0.003 in. thick was placed at x/c = 0.49 on the upper surface and x/c = 0.65 on the lower surface. This caused the $\alpha_{L=0}$ to shift 3 deg. Additionally, $C_{l,max}$ was reduced to 1.05 and occurred 1 deg. higher than for the clean airfoil. C_d increased slightly but remained relatively constant from α = -5 to 4 deg. Above 4 deg., C_d of the tripped airfoil increased dramatically. At α = 12 deg., the tripped airfoil C_d was about 500% higher than the clean airfoil C_d at the same angle of attack. These results are typical for extremely thick airfoil sections and similar effects have been observed in studies investigating the effects of surface roughness on wind turbine rotor blade root sections.[21]

Figure 6 also shows the effects of simulated ice on the mid-boot blade section performance. As one might expect in light of the tripped airfoil performance, simulated ice roughness causes remarkably severe degradation in the aerodynamic performance of the mid-boot blade section. For all three icing conditions, the shape of the lift curve for the iced mid-boot blade section is qualitatively different than for the clean and tripped cases. For runs 19A and 21, C_l decreases as angle of attack increases until moderate positive angles of attack. Beyond about 6 deg., C_l begins to increase with increasing angle of attack, but at a much reduced rate compared with the clean and tripped cases. Simulated ice also has a large effect on C_d, changing the angle of attack at which $C_{d,min}$ occurs and increasing drag at all angles of attack. $C_{d,min}$ increased from 0.0133 at α = 1 deg. for the clean airfoil to 0.0511 at α = -2 deg. for Run 3B, 0.0941 at α = 6 deg. for Run 19A, and 0.1107 at α = -6 deg. for Run 21. These values correspond to increases of 380%, 708%, and 832%, respectively, relative to the clean airfoil drag. The large reductions in C_l and increases in C_d are likely due in part to the 33% airfoil thickness. It is probable that surface contamination causes premature separation of the boundary layer, causing the airfoil to behave similar to a bluff body.

The effects of ice on the 50% and 75% blade sections are also shown in Fig. 6. The effects of ice on these blade sections are more typical of standard iced-airfoil experiments than was the case for the mid-boot section, likely because these airfoils are much thinner (9% and 6% thick). The 50% blade section had a $C_{l,max}$ nearly identical to the mid-boot section, but it occurred at 10 deg. instead of 12 deg. C_d was much lower for the 50% blade section, with $C_{d,min}$ = 0.0072 at α = 1 deg. Above α = 1 deg., C_d increased gradually with angle of attack. This is in contrast to the mid-boot section, which had a relatively constant C_d over the linear angle of attack range, a characteristic of thick airfoils. The effects of simulated ice on the 50% section were substantial, but not nearly as extreme as was the case for the mid-boot section. Simulated ice from Runs 3B, 19A, and 21 caused degradations in $C_{l,max}$ of 33.6%, 12.6%, and 52.1%, respectively. The stall angle of attack decreased from 10 deg. for the clean airfoil to 5 deg. for the simulated ice of Run 21, the worst case. Ice simulations causing the largest reductions in $C_{l,max}$ also caused the largest increases in C_d, with the simulation of Run 21 causing $C_{d,min}$ to increase by 800%.

The 75% blade section showed slightly less sensitivity to ice accretion than did the 50% blade section. The clean airfoil $C_{l,max}$ was lower, reaching only 1.09. $C_{d,min}$ was similar at 0.0074, but occurred 1 deg. later at α = 2 deg. As with the 50% blade section, the ice simulation of Run 21 caused the largest aerodynamic penalty, decreasing $C_{l,max}$ by 26% and increasing $C_{d,min}$ by nearly 700%. $C_{d,min}$ also occurred at a 3 deg. lower angle of attack than for the clean airfoil. The ice simulation of Run 19A had much smaller effects on $C_{l,max}$ and C_d. In fact, the value of $C_{l,max}$ did not change significantly, but instead the angle at which it occurred increased by at least 2 deg. $C_{d,min}$ increased by 120%, a small increase compared to that caused by the other ice simulations. The simulation of Run 3B caused penalties more severe than those of Run 19A but less severe than those of Run 21, decreasing $C_{l,max}$ by 11% and increasing $C_{d,min}$ by 350%.

For radial stations inboard of x = 0.50, the airfoil performance data of Fig. 6 corresponds roughly to conditions along the propeller blade at an advance ratio of J = 0.8 for a freestream velocity of 100 kts. These are the conditions at which Dumont et al.[1] collected ice accretion tracings and thrust data on a full-scale propeller. Beyond the x = 0.50 radial station, the local Mach number seen by each blade section exceeds the maximum Mach number capability of the Illinois' wind tunnel (M_{max} = 0.3). For these conditions, the local Mach number at the 75% blade station is 0.48. Since higher Mach number data were not available, airfoil performance data for M = 0.30 were used.

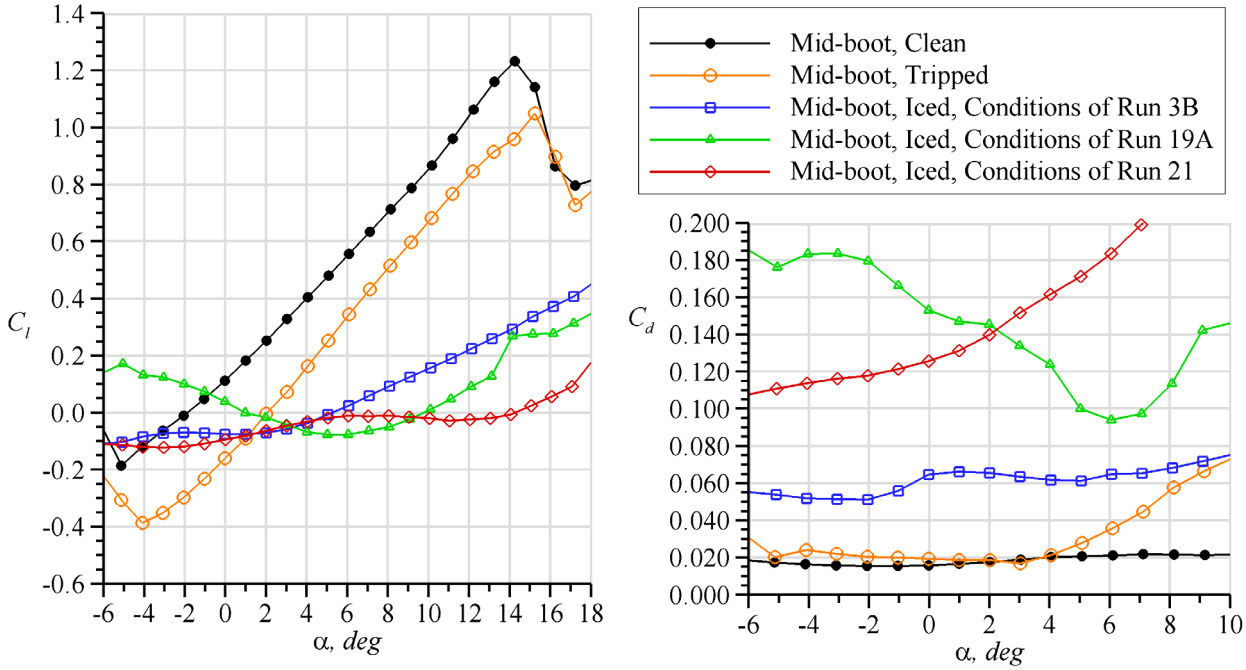
Mid-boot, Clean
Mid-boot, Tripped
Mid-boot, Iced, Conditions of Run 3B
Mid-boot, Iced, Conditions of Run 19A
Mid-boot, Iced, Conditions of Run 21
C_l
α, deg
C_d
α, deg

(a)

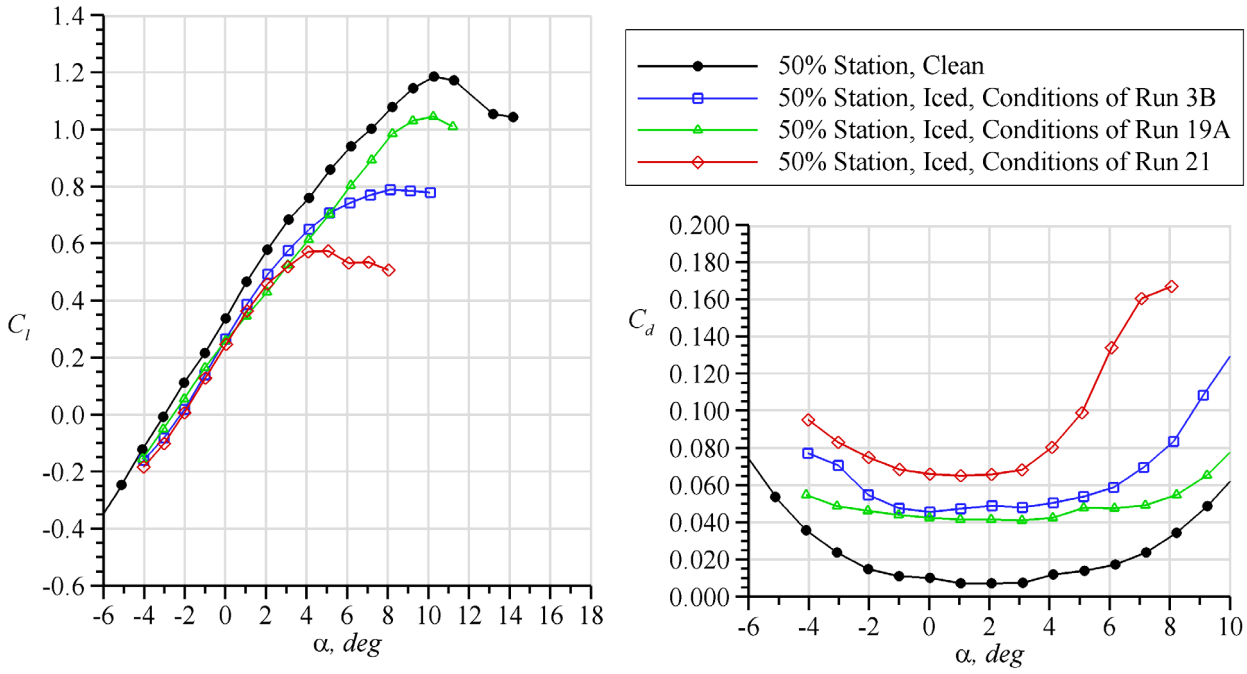
50% Station, Clean
50% Station, Iced, Conditions of Run 3B
50% Station, Iced, Conditions of Run 19A
50% Station, Iced, Conditions of Run 21
C_l
α, deg
C_d
α, deg

(b)

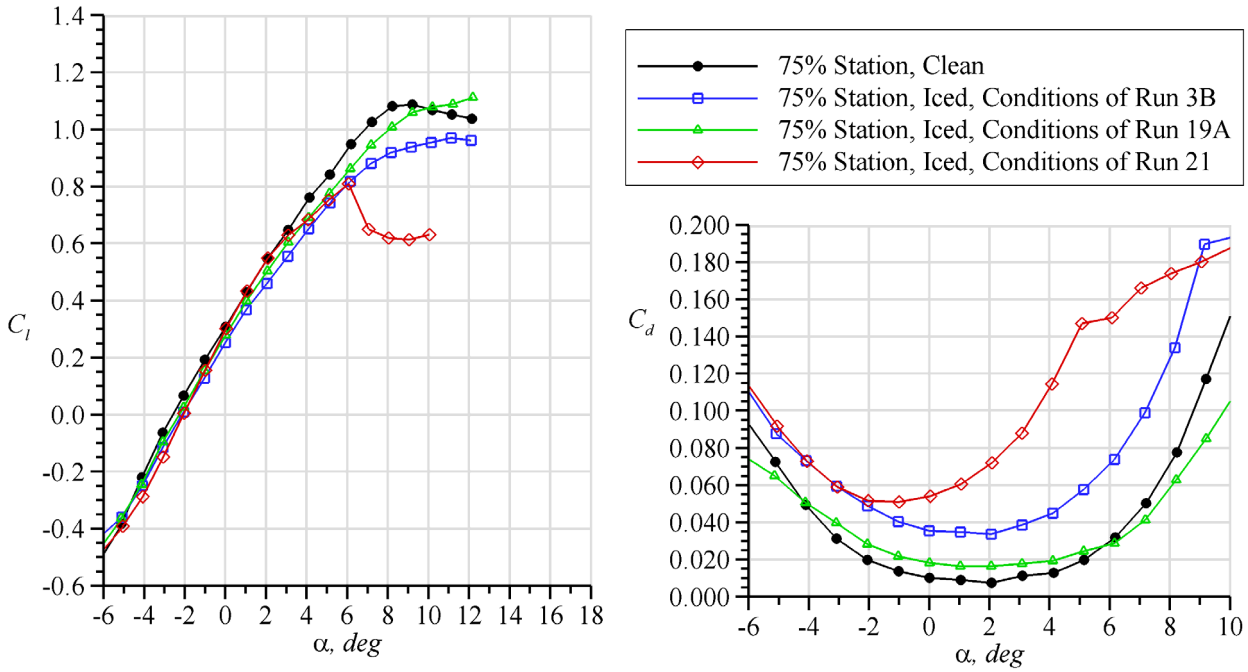

(c)

Fig. 6 Aerodynamic performance data for the (a) 25% (mid-boot), (b) 50% station, and (c) 75% station propeller blade sections, clean and iced. The mid-boot data were obtained at M = 0.2, Re = 600,000 and the 50% and 75% blade section data were obtained at M = 0.3, Re = 900,000.

Propeller Performance Code Calculations

Once clean and iced blade section aerodynamic performance data were obtained, they were used as inputs (along with chord and twist distributions for the propeller) into the propeller performance code discussed earlier in this paper. The predictions of the code were compared with experimental data obtained from the test of a full-scale propeller in the McKinley Climatic Laboratory, also discussed earlier in this paper. These comparisons are now discussed.

For each of the conditions of runs 3B, 19A, and 21 (shown in Table 1), iced propeller C_T, C_P, and η were compared with the corresponding clean, baseline case. These comparisons are shown in Fig. 7 - Fig. 11. The experimental data for these comparisons were obtained at a single advance ratio, and are shown as a single point in the figures. For the propeller code predictions, tripped airfoil data for the 25% blade section at $x = 0.25$ was used to estimate clean propeller performance, as this section showed high sensitivity to contamination and was unlikely to have been operating in a purely "clean" state. Note that for both experimental and computational data there are minor variations in clean propeller performance for each run condition. This is due to small differences in ambient temperature and propeller RPM and pitch setting, and in the case of experimental data, experimental uncertainty.

Data for the conditions of run 3B are shown in Fig. 7. The propeller performance code shows C_T and C_P to decrease with increasing advance ratio. It slightly under-predicts clean C_T by about 8% and C_P by 2% compared to the experimental data. As a result, the code predicts propeller efficiency (computed $\eta = J^*C_T/C_P$) to be about 6% below that which was measured experimentally. Despite this minor disagreement in clean propeller performance, the predicted and measured effects of ice accretion are similar. The computational data, labeled "Code, Iced, Run 3B" in Fig. 7, are shown over a range of advance ratios. Both the experimental and computational data show C_T to decrease and C_P to remain almost constant for the iced case, corresponding to a decrease in propeller efficiency when ice has accreted. The magnitudes of these decreases are shown in Fig. 8. During the McKinley test, a thrust decrease of 6% and power decrease of 1% was recorded for the conditions of run 3B. The propeller performance code predicted decreases of 11% and 5%, respectively, at the same advance ratio of $J = 0.82$.

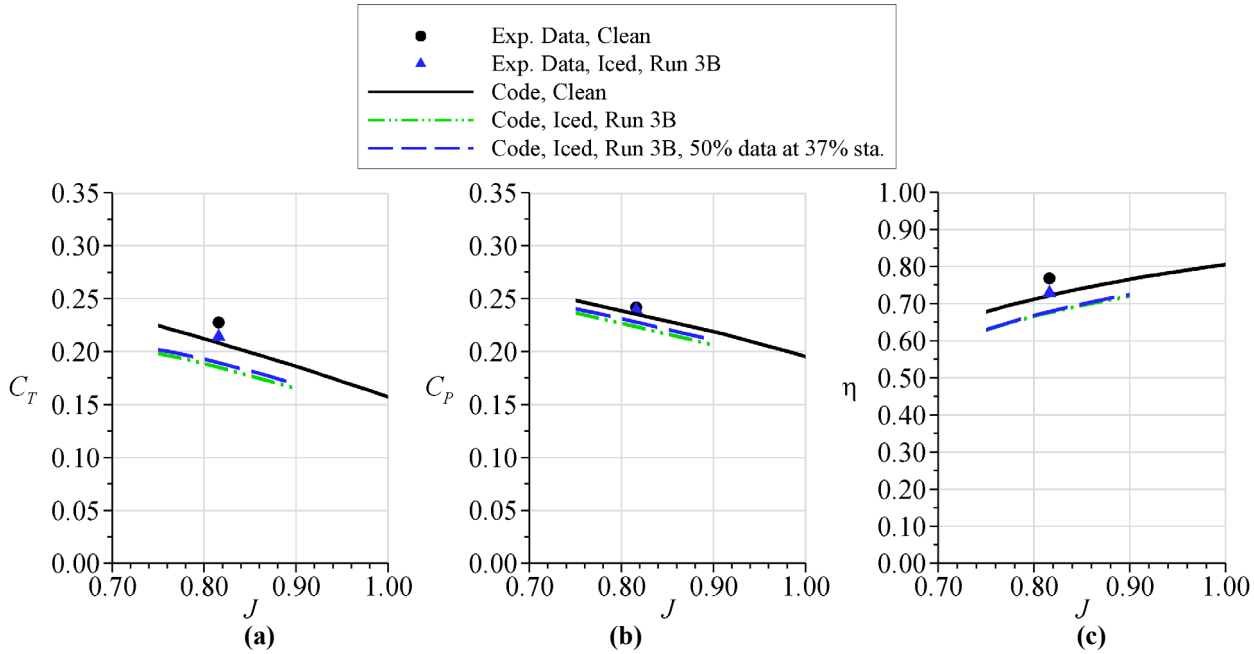

Fig. 7 Comparison between predicted and measured propeller performance degradation due to icing conditions of Run 3B. Effect of ice accretion on (a) thrust coefficient, (b) power coefficient, and (c) propeller efficiency.

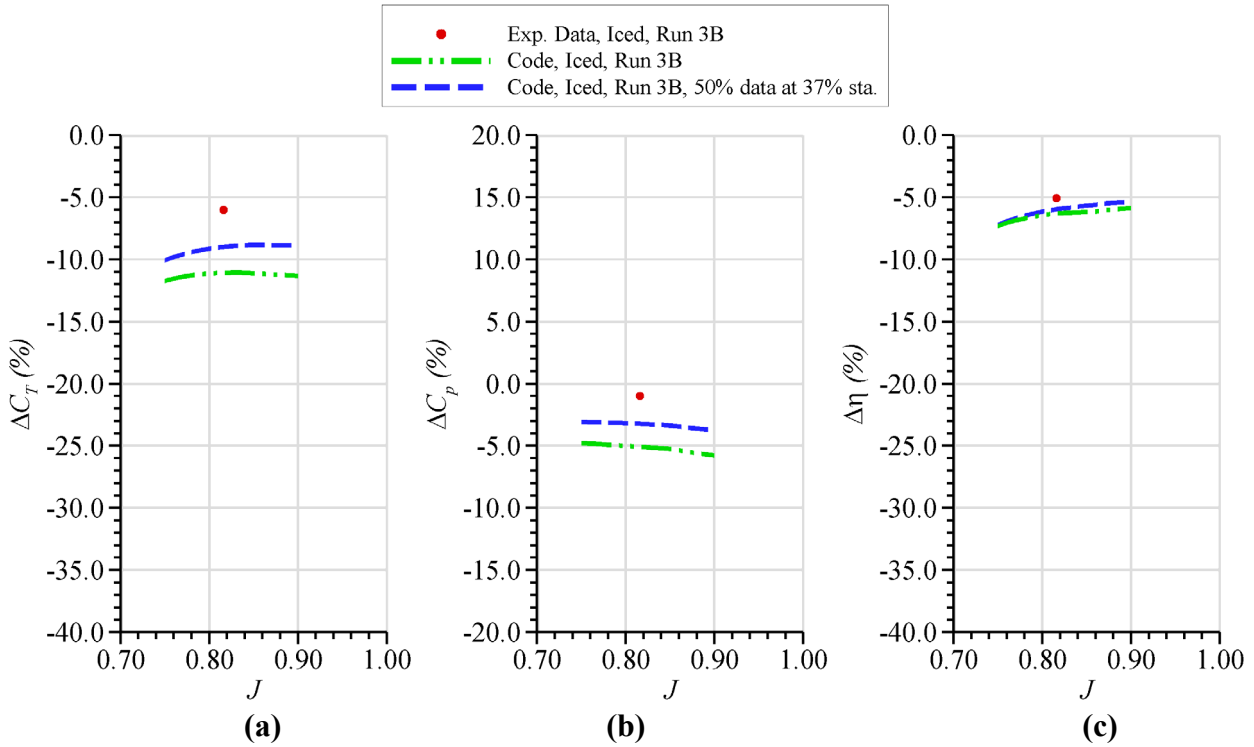

Fig. 8 Reduction in (a) thrust coefficient, (b), power coefficient, and (c) propeller efficiency due to ice accreted under the conditions of run 3B.

Because the 25% blade section had extremely poor performance when iced, the input to the propeller performance code was modified to reduce its influence. The propeller code interpolates the performance data linearly from the 25% to the 50% station and the 25% station data were considered to unrepresentatively skew the

performance interpolation. Therefore, a sensitivity study was conduct in which an additional blade station was added at 37% to modify the interpolation. The data used for this blade section was the run 3B 50% blade station data from Fig. 6(a). As a result of this modification, the code assumed constant blade section properties (of the iced 50% station) from $x = 0.37$ to $x = 0.50$; the 25% station data had no influence over this range. These adjusted data are labeled "Code, Iced, Run 3B, 50% data at 37% sta." in Fig. 7 and Fig. 8. The figures show that this helped to improve agreement between experimental and predicted performance degradation. With this modified input data, the propeller performance code predicted thrust and power decreases of 9% and 3%. The propeller efficiency, η, was similar to the original run 3B code predictions because the difference in C_T and C_P approximately canceled out. This example suggests that linear interpolation between the 25% and 50% blade stations may be insufficient to accurately predict propeller performance in some cases. To improve accuracy, more blade section data may be necessary or a more sophisticated interpolation routine should be used.

Propeller performance code predictions for the conditions of run 19A are shown in Fig. 9. Unlike run 3B, C_P increased when ice was accreted. Recall that the power coefficient, C_P, corresponds to input power provided to the propeller. It is not inconsistent for ice to have caused an increase in C_P for the conditions of run 19A and a decrease for the conditions of run 3B. In both cases, ice accretion caused blade section C_l to decrease and C_d to increase. According to eqn. 2, a decrease in C_l corresponds to a decrease in dC_P, and an increase in C_d corresponds to an increase in dC_P. Thus, the ultimate effect on C_P depends on exactly how blade section C_l and C_d are affected, which varies by accretion. In contrast, C_T almost always decreases with ice accretion, and this was the case for the conditions of run 19A. Equation 1 shows that as C_l decreases and C_d increases, as is the case with ice accretion, dC_T (and therefore C_T) decreases. Thus, for the conditions of run 19A, more input power was required to generate a smaller amount of output thrust, reducing propeller efficiency. The changes in C_T, C_P, and η for run 19A are shown in Fig. 10. Agreement between computational data and experiment is good. The propeller code predicts a reduction in thrust of 8% and a reduction in efficiency of 9%, compared with experimentally measured reductions of 9% in both thrust and efficiency. Similarly, the code predicts a 2% increase in C_P, in good agreement with the measured 1% increase.

Also shown in Fig. 9 and Fig. 10 are the predictions of the propeller performance code when data for a fourth blade section was input at a radial station of $x = 0.37$. The data used at this station were that of the 50% blade section for the icing conditions of run 19A. The intent of this run was to determine the effects of interpolation between the 25% and 50% blade stations in a similar manner to what was done for run 3B. The addition of the fourth station caused both C_T and C_P to increase relative to the case in which only three blade stations were used (Fig. 9). This caused a smaller predicted reduction in thrust and a larger predicted increase in power required, resulting in worse agreement with experiment (Fig. 10). This contrasts with the case of run 3B, in which the addition of blade section data at the 37% station improved agreement. These results indicate that simply incorporating the 50% blade section data at the 37% station does not consistently improve agreement with experiment, and this method should not be used in place of obtaining aerodynamic performance data at more than three radial stations.

The SLD conditions of run 21 produced ice accretions larger than observed for the other two runs. Accordingly, iced C_T and η were both measured to be much lower than the clean propeller C_T and η (Fig. 11). C_P, however, was measured to be the same in both the iced and clean cases. Note that experimental data obtained for the conditions of run 21 was actually obtained from run 21C, for which the conditions were very similar. The large accretions generated during the SLD conditions of run 21 introduced additional challenges in properly predicting propeller performance degradation, as shedding effects were more significant for this run.

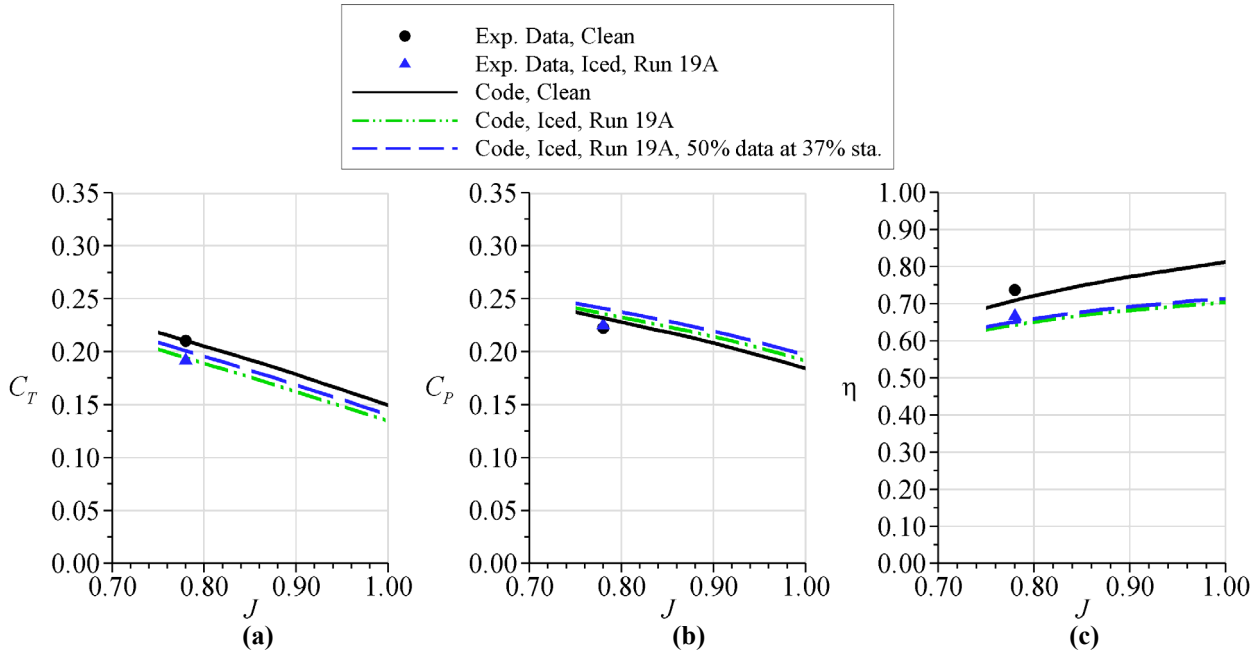

Fig. 9 Comparison between predicted and measured propeller performance degradation due to icing conditions of Run 19A. Effect of ice accretion on (a) thrust coefficient, (b) power coefficient, and (c) propeller efficiency.

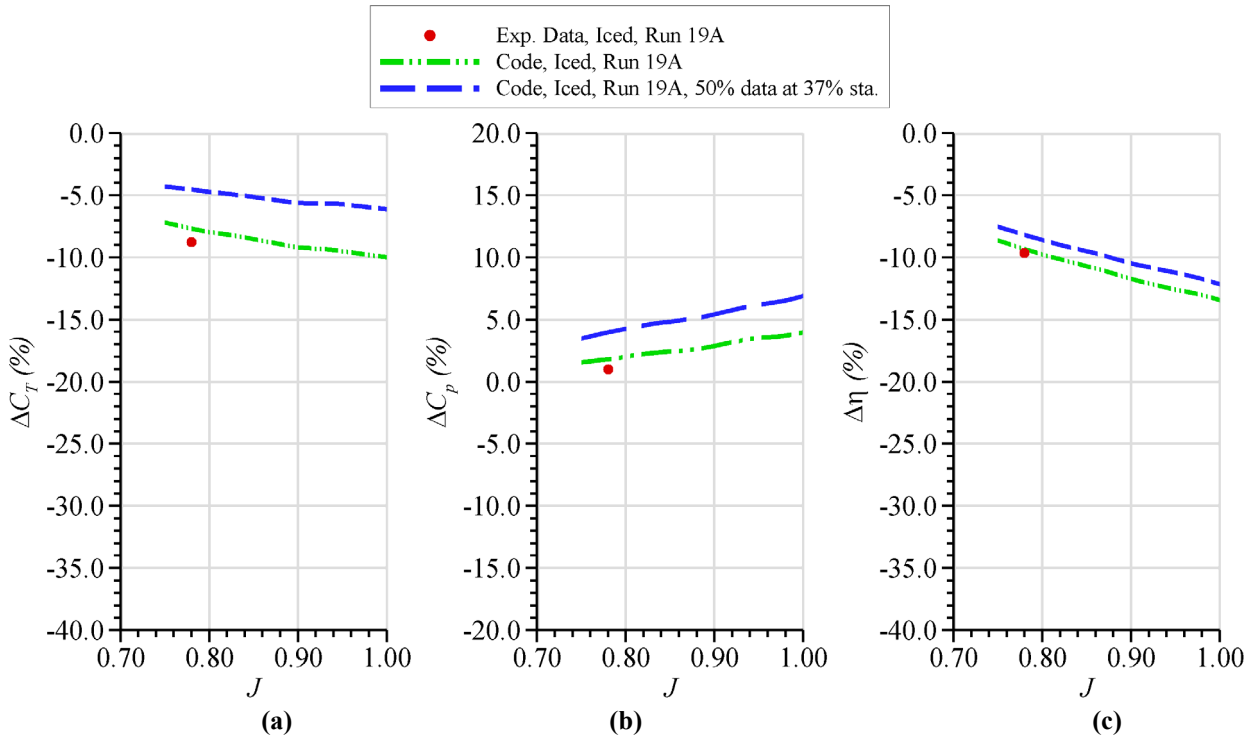

Fig. 10 Reduction in (a) thrust coefficient, (b), power coefficient, and (c) propeller efficiency due to ice accreted under the conditions of run 19A.

The data discussed thus far generated by the propeller performance code used the blade section data shown in Fig. 6, which implicitly assumes that no ice accretion or shedding occurred in the McKinley test between the time the propeller thrust was recorded and the time at which the tracing was made and also that the ice simulations used were representative of the ice on all propeller blades. However, ice shedding may have occurred after thrust was

recorded, or even a small amount of ice may have accreted after the thrust measurement but prior to the icing cloud being turned off. This introduces uncertainty into the ice accretion geometries shown in the tracings, which may result in more or less severe aerodynamic penalties than estimated from the Illinois wind tunnel tests. Stop-action video from the McKinley test was used to gauge the extent to which shedding occurred near the end of the test. According to the video, ice was shed from the 75% station on some of the blades near the end of the run, around the time that thrust was recorded. At this time, each of the propeller blades had differing amounts of ice, depending on the extent to which shedding had occurred and exactly when it occurred. To gauge the magnitude of these effects, a second run was conducted using the propeller performance code which assumed ice had shed from the 75% station. Instead of using the iced data of run 21 shown in Fig. 6(c), iced blade section data from run 19A were input to the code for use at the 75% station. The accretion of run 19A was much smaller than that of run 21 and appeared to resemble the ice remaining on the propeller blade after a shed had occurred. Note that this model effectively assumed that ice shedding occurred on all four blades, rather than just some of the blades, and the model which assumed no shedding assumed that no shedding occurred on any of the blades. The propeller performance code currently has no provision for assuming different amounts of ice accretion (or for that matter, differing aerodynamic performance) on each of the blades, and this should be considered when interpreting the results.

The predictions of the propeller code on C_T, C_P, and η are shown in Fig. 11. Both the "no shedding" and "shedding" models predicted reductions in thrust and efficiency due to ice accretion. As would be expected, predictions of iced C_T using the shedding model tended to be closer to predicted values for the clean propeller than the model of the propeller which assumed no shedding. The "no shedding" model predicted a C_T reduction of 24% for the conditions of run 21, compared with a reduction of 21% predicted by the shedding model (Fig. 10). The experimentally measured thrust reduction fell in between at 22%. In contrast, the two models predicted very different values of C_P. The model which assumed no shedding predicted C_P 10% above the clean propeller C_P, and the model which assumed shedding predicted C_P 7% below the clean C_P. These results show that ice shedding can have a measurable effect on the magnitude of the degradation of propeller performance, especially with regard to C_P, and appropriate models should be developed.

The effects of ice accretion on propeller performance can be better interpreted by examining the blade section performance at various stations along the propeller blade. For example, Fig. 13 shows blade section performance for each radial station along the propeller blade for the SLD conditions of Run 21. Recall that the performance of only three stations (25%, 50%, and 75%) was experimentally measured. These data were interpolated to obtain the smooth curves shown in Fig. 13. In the figure, data for both shedding models are shown, and are in agreement up to $x = 0.50$ because they use the same data at the mid-boot and 50% station. Recall that the model which assumed ice shedding to have occurred at the 75% station uses data from run 19A at this station, while the model which assumes no shedding to occur uses data from run 21 (Fig. 6). Note that the large differences seen in the α and C_l distributions between the iced and clean cases below $x = 0.5$ result largely from the tremendous sensitivity of the mid-boot section to surface roughness. For the iced case of Run 21, C_l of the mid-boot section ranges from -0.1 to 0 at the local geometric angle of attack seen by the inboard portion of the propeller blade. This significantly biases the value of C_l interpolated from $x = 0.25$ to 0.50, as C_l is seen to increase almost linearly from $x = 0.25$ to $x = 0.50$. It is also responsible for the very low induced angle of attack in this range, which causes an increase in effective angle of attack inboard of $x = 0.50$. The poor performance of the mid-boot section in icing conditions affects the C_d distribution in a similar way. At $x = 0.25$, C_d is 400% higher in the iced case than the clean case. Beyond $x = 0.50$, the two shedding models diverge since they used different blade section aerodynamic performance data at the 75% station. The shedding model causes a slight increase in C_l and a large decrease in C_d outboard of x = 0.50 relative to the model which assumes no shedding.

The incremental power coefficient (dC_P) distribution is only slightly lower in the iced case than the clean case up to $x = 0.5$, despite the much higher drag of the inboard portion of the blade. This is partly due to the much lower speed of the propeller blade at inboard stations and partly due to the greater sensitivity of dC_P to propeller blade lift distribution. Outboard of $x = 0.50$, the propeller blade sees much higher local velocities, so increases in C_d have a larger effect on dC_P. This is especially evident in comparing the models with and without shedding, as C_l is similar between the two cases but C_d is drastically different. As would be expected from the C_d distribution, for the model with no shedding there is a large increase in dC_P outboard of $x = 0.50$ relative to the model which assumes shedding to have occurred (and also the clean model). The incremental thrust coefficient (dC_T) is lower in the iced case than the clean case at all propeller blade stations. At the inboard stations, this is caused by the very low lift and very high drag of the mid-boot section. At outboard stations, C_l is slightly less for the iced blade sections relative to the clean blade sections at the relevant angles of attack and C_d is much higher in the iced case. Decreased values of C_l and increased values of C_d cause decreased values of dC_T (this also explains the differences in dC_T existing between the "shedding" and "no shedding" models). The incremental propeller efficiency ($d\eta$) distribution is also shown in Fig.

13 and is proportional to dC_T/dC_P. When dC_T decreases and dC_P increases, as is the case for the iced propeller, dη drops drastically. The large difference in dη between the "shedding" and "no shedding" models outboard of x = 0.50 results mainly from the large decrease in C_d as ice is shed at the 75% station.

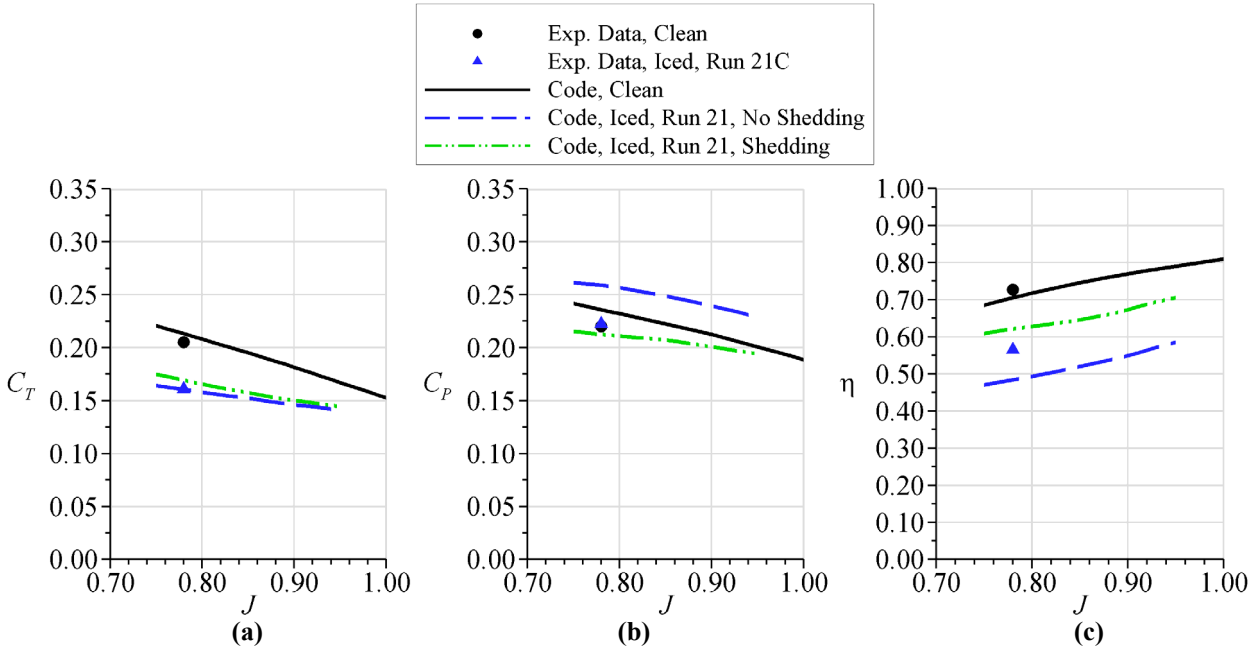

Fig. 11 Comparison between predicted and measured propeller performance degradation due to icing conditions of Run 21. Effect of ice accretion on (a) thrust coefficient, (b) power coefficient, and (c) propeller efficiency.

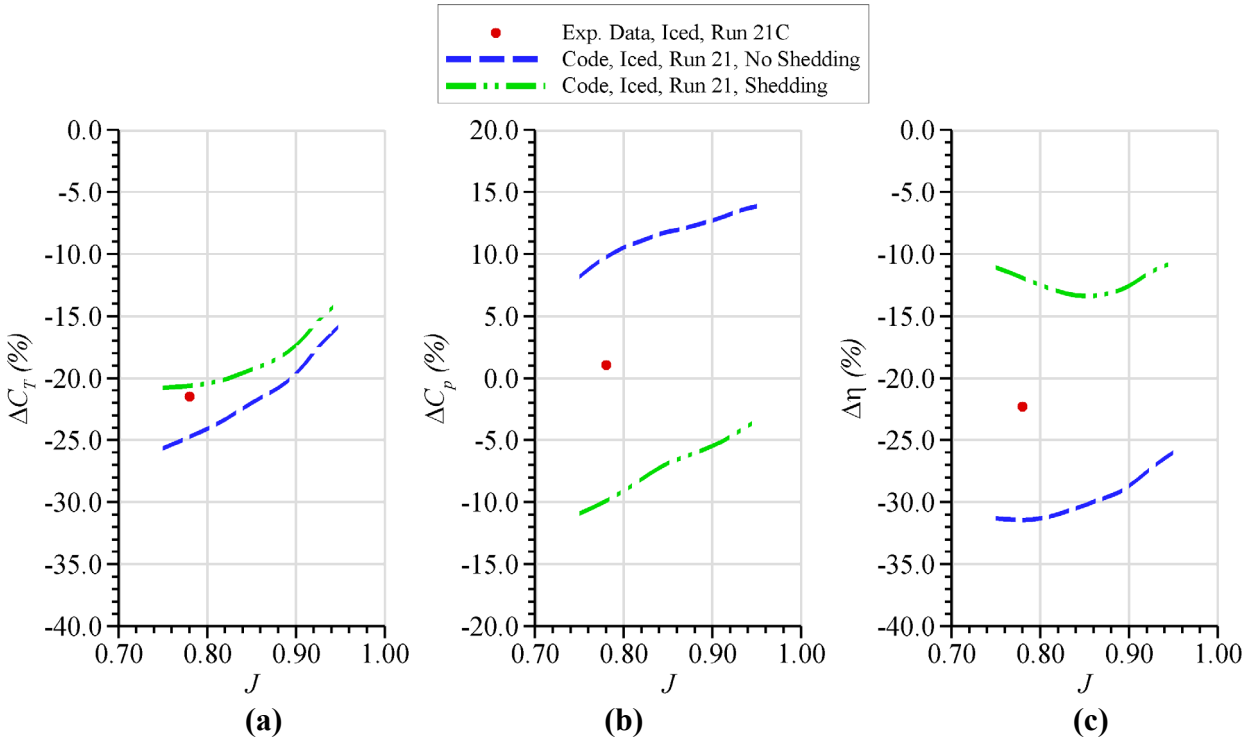

Fig. 12 Reduction in (a) thrust coefficient, (b), power coefficient, and (c) propeller efficiency due to ice accreted under the conditions of Run 21.

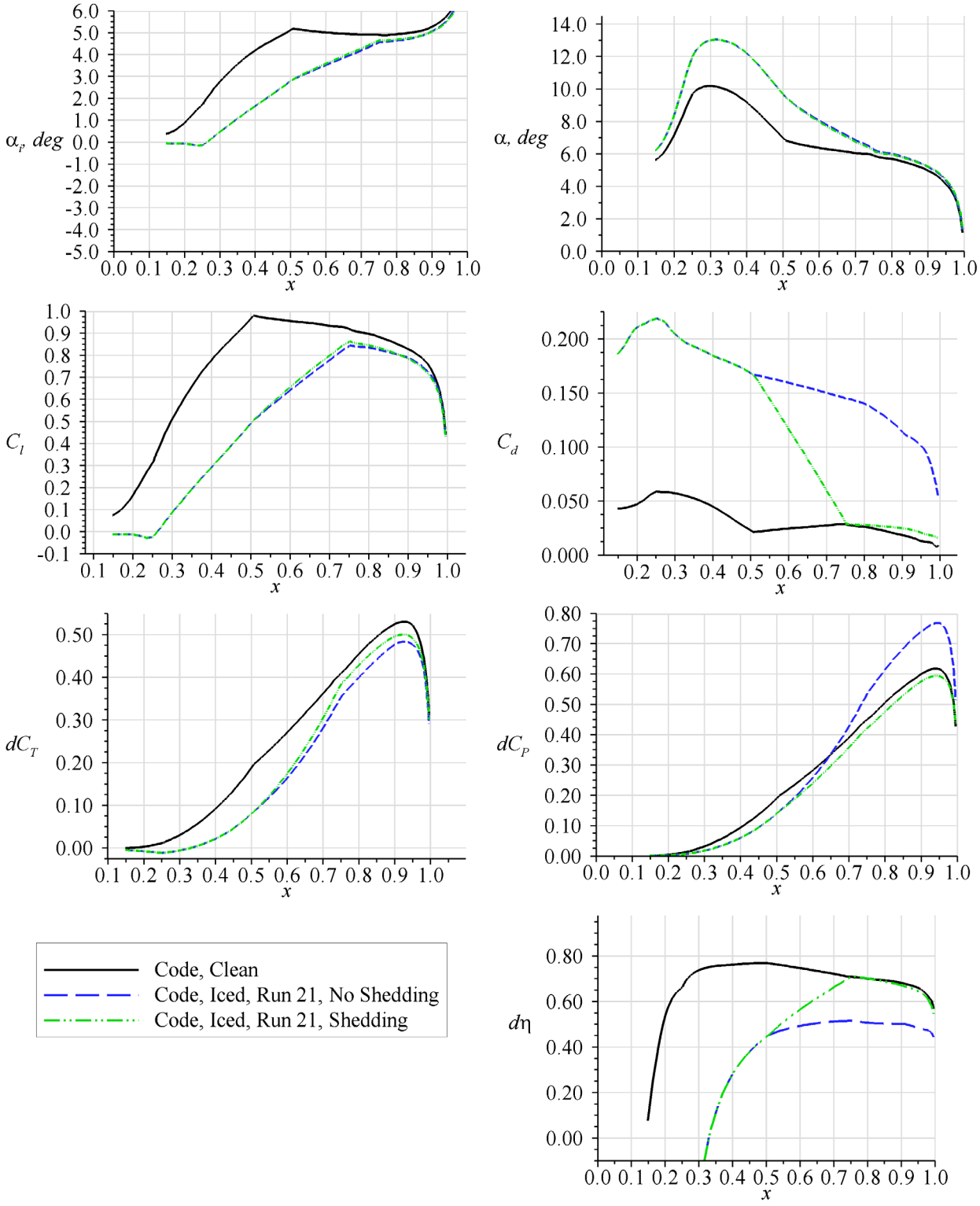

Fig. 13 Predicted blade section properties along the propeller blade at an advance ratio of J = 0.78 for the SLD conditions of run 21. The properties are shown using two models: one which assumed no shedding and one which assumed ice was shed at the 75% station.

Mach Number Considerations

The results of the propeller performance code discussed above use airfoil performance data taken at M = 0.2 for the 25% blade section and at M = 0.3 for the 50% and 75% blade sections. This was reasonable for the 25% and 50% blade sections, as the actual Mach number seen by those blade sections during the McKinley test were 0.22 and 0.36. The 75% blade section, on the other hand, saw Mach numbers around 0.48 in the McKinley test. No data could be obtained at this high of a Mach number because the Illinois wind tunnel was limited to a maximum Mach number of 0.3. For the iced conditions, this likely had only a very small effect, as airfoil sensitivity to variations in Mach number is reduced considerably when iced.[22] As discussed earlier, there is also a large degree of uncertainty in iced blade section aerodynamic performance due to ice shedding effects, and the uncertainty due to Mach number is much smaller. In the case of the clean 75% blade section performance, on the other hand, Mach number effects may have been more significant. Above M = 0.3, the effects of increasing Mach number are to increase section lift curve slope and decrease $C_{l,max}$. In most cases, the 75% blade section operates well below $C_{l,max}$, so the main effect of using higher Mach number data would likely be a slight increase in predicted clean propeller C_T and perhaps C_P. For the case of the in-flight propeller, the Mach number was much greater than during the McKinley test, having values near 0.4 at the 25% station and in excess of 0.6 at the 75% station. To accurately model the propeller during in-flight conditions, higher Mach number data should be used. The next phase of this study is to use the ice accretion prediction code LEWICE to computationally determine ice geometries due to the conditions of runs 3B, 19A, and 21. The aerodynamic performance of each iced blade section with the appropriate LEWICE geometry will then be analyzed using a 2-D RANS code, such as Fluent.[23] During this process, higher Mach number data will be generated and used so that more appropriate Mach numbers can be used to generate the in-flight propeller performance.

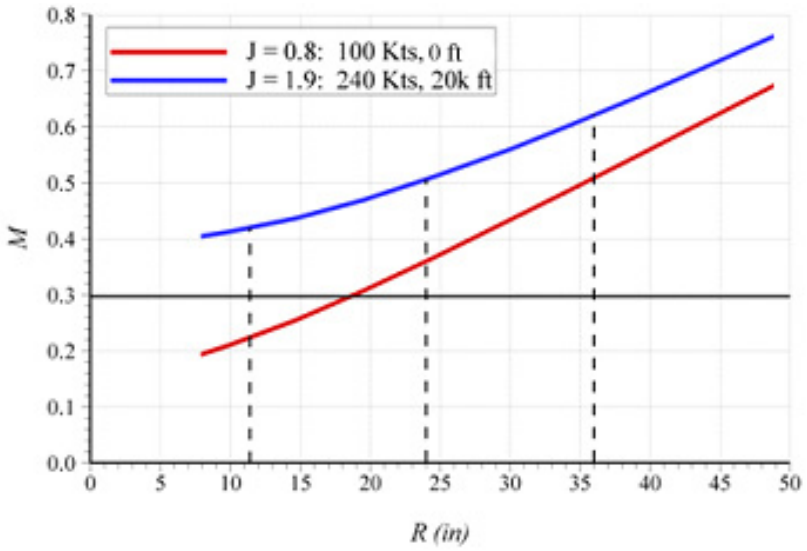

Fig. 14 Local Mach number seen by the propeller blade at various stations for the conditions of the McKinley test (J = 0.8) and those which would be seen in flight. Mach numbers corresponding to the 25% (R = 11.5 in), 50% (R = 24 in), and 75% stations (R = 36 in) are shown by dashed vertical lines.

Conclusions

The objective of the current study was to develop a methodology to analyze propeller performance in icing conditions. The accuracy of this method was quantified using data from a full-scale propeller icing test recently conducted at the McKinley Climatic Laboratory in which propeller thrust was measured and propeller ice accretion documented. The method employed to predict iced-propeller performance had three primary steps:

1) Using ice accretion data from the McKinley test, 2-D ice simulations were built for the 25%, 50%, and 75% propeller blade stations and the aerodynamic performance of each blade section (clean and iced) was measured in the Illinois wind tunnel

2) These section aerodynamic performance data were input into a blade-element/vortex theory propeller performance code to determine the effect of ice accretion on propeller performance
3) The degradations in performance predicted by the code were compared with thrust data recorded during the McKinley test to quantify the accuracy of the method.

Predictions of the clean propeller performance were only in fair agreement with experimentally measured values of thrust. This may in part have been due to the use of lower Mach number data at the 75% station than was actually seen by the blade, or perhaps due to the use of aerodynamic data for only three blade sections in the blade element code. It was found that the effect of ice accretion on C_P was small compared to the reductions in thrust and efficiency. Depending on the ice accretion, C_P either increased or decreased slightly when ice was accreted. Predictions of the reductions in C_T and η were in reasonably good agreement with experimentally measured reductions for the smaller accretions of the App. C conditions, though accuracy may be improved by using more blade section data between the 25% and 50% stations or using a more sophisticated interpolation routine. Another consideration when comparing the results of the propeller code with experiment is uncertainty in the experimental data. The net force on the propeller and thrust stand were measured using a load cell, and the isolated propeller thrust was calculated using a rough correction to account for drag on the thrust stand. In all cases investigated, ice accretion on propeller blades caused reductions in thrust and efficiency. For the SLD icing conditions, the ice accretions tended to be much larger than for the App. C conditions, and shedding of ice from the propeller blades was found to be especially prevalent at outboard blade stations. Therefore, the propeller performance code was also operated using a model which assumed shedding consistent with that observed in stop-action video of the McKinley icing test. As would be expected, when a simple shedding model was included reductions in propeller performance were much less severe. Predictions of efficiency loss due to SLD conditions ranged from 10% to 31% depending on the extent to which ice was shed. The experimentally measured reduction in efficiency was 23%. Similarly, the experimentally measured changes in C_T and C_P were bracketed by the predictions of the propeller code. The predicted reduction in C_T was too large when no shedding on any blade was assumed and too small when 75% blade section shedding on all blades was assumed. Likewise, the shedding model predicted an increase in C_P while C_P was predicted to decrease with the assumption of no shedding; experimental measurements showed little change in C_P. For determining the effects of significant ice accretion (such as that which occurs in SLD conditions) on propeller performance, it is recommended that an improved shedding model be used in conjunction with the propeller performance code.

Future work will focus on using LEWICE to predict the ice accretion geometry which forms on the 25%, 50%, and 75% blade sections. Stop-action video of the propeller blades obtained during the McKinley test will be used to help account for ice shedding and guide the LEWICE predictions. If appropriate, LEWICE may also be used to predict ice geometries for additional blade sections. The effect of the LEWICE-predicted geometries on blade section performance will then be computed using a 2-D RANS code, such as Fluent. These data can be compared with the experimental blade section aerodynamic performance data obtained during the Illinois wind tunnel test and discussed in this paper. At this point, Mach number effects can be better assessed, as the Illinois wind tunnel data was limited to M = 0.3 whereas the Fluent data can be obtained at more representative Mach numbers. The Fluent data will then be input into the propeller performance code in place of the Illinois data to predict propeller performance. Outputs of the code will be compared with experimentally measured changes in propeller performance, as was done in this paper, to quantify the accuracy of the method. If successful, propeller performance degradation in icing conditions can be predicted to a known degree of accuracy using entirely computational methods, although it is likely that an ice shedding model will also need to be developed and employed to appropriately account for shedding effects.

Acknowledgments

This work was supported by the Federal Aviation Administration (FAA) Office of Aviation Research under the grant DTFA 96-G-023. From the FAA, the authors wish to thank Jim Riley, the contracting officer's technical representative, and Chris Dumont, who provided valuable advice about the testing at McKinley. Thanks also go to Dominik Krug, from the Technische Universität Darmstadt, who wrote the propeller performance code while at the University of Illinois, and to Austin Ellis at the University of Illinois.

References

[1] Dumont, C., Pellicano, P., Smith, T., and Riley, J., "Results From a Full-Scale Propeller Icing Test," AIAA Paper 2008-0432, *46th AIAA Aerospace Sciences Meeting & Exhibit*, Reno, NV, Jan. 2008.

[2] Corson, Jr., B.W., and Maynard, J.D., "The Effect of Simulated Icing on Propeller Peformance," NACA TN-1084, Jul. 1946.

[3] Preston, G.M., and Blackman, C.C., "Effects of Ice Formations on Airplane Performance," NACA TN-1598, May 1948.

[4] Neel, Jr., C.B., and Bright, L.G., "The Effect of Ice Formations on Propeller Performance," NACA TN-2212, Oct. 1950.

[5] Korkan, K.D., Dadone, L., Shaw, R.J., "Performance Degradation of a Propeller System Due to Rime Ice Accretion," *J. Aircraft*, v. 21, n. 1, 1984, pp. 44-49.

[6] Miller, T.L., Korkan, K.D., and Shaw, R.J., "Analytical Determination of Propeller Performance Degradation due to Ice Accretion," *J. Aircraft*, v. 24, n. 11, 1987, pp. 768-775.

[7] Bragg, M.B., "Rime Ice Accretion and Its Effect on Airfoil Performance," NASA CR 165599, Mar. 1982.

[8] Gray, V.H., "Prediction of Aerodynamic Penalties Caused by Ice Formations on Various Airfoils," NASA TN-D 2166, Feb. 1964.

[9] Flemming, R.J., and Lednicer, D.A., "High Speed Ice Accretion on Rotorcraft Airfoils," NASA CR 3910, Aug. 1985.

[10] Reichhold, J., Bragg, M., and Sweet, D., "Experimental Determination of the Droplet Impingement Characteristics of a Propeller," AIAA Paper 97-0179, *35th AIAA Aerospace Sciences Meeting & Exhibit*, Reno, NV, Jan. 1997.

[11] Farag, K.A., and Bragg, M.B., "Three Dimensional Droplet Trajectory Code for Propellers of Arbitrary Geometry," AIAA Paper 98-0197, *36th AIAA Aerospace Sciences Meeting & Exhibit*, Reno, NV, Jan. 1998.

[12] Timmons, L., "Icing Investigations and Product Development on MU-2B Airplanes," SAE 2003-01-2088, FAA In-Flight Icing/Ground De-icing International Conference, Chicago, IL, Jun. 2003.

[13] McCormick, B.W., *Aerodynamics, Aeronautics, and Flight Mechanics*, 2nd Ed., John Wiley & Sons, 1995.

[14] Krug, D., "Development of a Propeller Performance Code," Independent Study Rept., Technische Universität Darmstadt and University of Illinois, Jun. 2008.

[15] Drela, M., "XFOIL: An Analysis and Design System for Low Reynolds Number Airfoils," Jun. 1989.

[16] Busch, G., Broeren, A., and Bragg, M., "Aerodynamic Simulation of a Horn-ice Accretion on a Subscale Model," AIAA Paper 2007-0087, *45th AIAA Aerospace Sciences Meeting & Exhibit*, Reno, NV, Jan. 2007.

[17] Broeren, A.P., Busch, G.T., and Bragg, M.B., "Aerodynamic Fidelity of Ice Accretion Simulation on a Subscale Model," SAE Paper 2007-01-3285, *2007 SAE Aircraft and Engine Icing International Conference*, Seville, Spain, Sep. 2007.

[18] Busch, G., Broeren, A., and Bragg, M., "Aerodynamic Fidelity of Two-Dimensional Subscale Ice Accretion Simulations," AIAA Paper 2008-7062, *26th AIAA Applied Aerodynamics Conference*, Honolulu, HI, Aug. 2008.

[19] Bragg, M., Broeren, A., Addy, H., Potapczuk, M., Guffond, D., and Montreuil, E., "Airfoil Ice-Accretion Aerodynamics Simulation," AIAA Paper 2007-0085, *45th AIAA Aerospace Sciences Meeting & Exhibit*, Reno, NV, Jan. 2007.

[20] Blumenthal, L.A., Busch, G.T., Broeren, A.P., and Bragg, M.B., "Issues in Ice Accretion Aerodynamic Simulation on a Subscale Model," AIAA Paper 2006-0262, *44th AIAA Aerospace Sciences Meeting & Exhibit*, Reno, NV, Jan. 2006.

[21] Van Rooij, R.P.J.O.M. and Timmer, W.A., "Roughness Sensitivity Considerations for Thick Rotor Blade Airfoils," *Journal of Solar Energy Engineering*, Vol. 125, Issue 4, Nov. 2003, pp. 468 – 478.

[22] Broeren, A.P. Bragg, M.B., Addy, Jr., H.E., Lee, S., Moens, F., and Guffond, D., "Effect of High-Fidelity Ice Accretion Simulations on the Performance of a Full-Scale Airfoil Model," AIAA-2008-0434, *46th Aerospace Sciences Meeting & Exhibit*, Reno, NV, Jan. 2008.

[23] FLUENT Version 6.1 Manual. Creare, Inc., Hanover NH.